

Bethe lattice approach study of the mixed spin- $\frac{1}{2}$ and spin- $\frac{7}{2}$ Ising model in a longitudinal magnetic field

S. Eddahri¹, M. Karimou², A. Razouk^{1,3}, F. Hontinfinde^{2,4*}, A. Benyoussef^{5,6}

¹ Material Physics Laboratory, Faculty of Sciences and Technology, Sultan Moulay Slimane University, Morocco

² Institute of Mathematics and Physical Sciences (IMSP), Republic of Benin

³ Department of Physics, Polydisciplinary Faculty, Sultan Moulay Slimane University, Morocco

⁴ University of Abomey-Calavi, Department of Physics, Republic of Benin

⁵ LMPHE, Faculty of Sciences, Mohammed V University, Rabat, Morocco

⁶ Hassan II Academy of Sciences and Technology, Rabat, Morocco

Received December 19, 2017, in final form February 7, 2018

The magnetic properties of the mixed spin- $\frac{1}{2}$ and spin- $\frac{7}{2}$ Ising model with a crystal-field in a longitudinal magnetic field are investigated on the Bethe lattice using exact recursion relations. The ground-state phase diagram is constructed. The temperature-dependent one is displayed in the case of uniform crystal-field on the $(k_B T/|J|, D/|J|)$ plane in the absence of the external constraint for lattice coordination numbers $z = 3, 4, 6$. The order parameters and corresponding response functions as well as the internal energy are calculated and examined in detail in order to feature the real nature of phase boundaries and corresponding temperatures. The thermal variations of the average magnetization are classified according to the Néel nomenclature.

PACS: 75.10.Hk, 75.10.Dg, 05.70.Fh, 05.50.+q

Key words: *Ising model, magnetization, response function, free energy, phase diagram, second-order transition*

1. Introduction

The investigation of mixed Ising systems has been of great interest in statistical mechanics during the past decades [1–4]. This is due to the revelation of novel critical magnetic properties not detected during studies of their single-spin counterparts. These systems are used to model ferrimagnetic materials whose properties are often needed in modern sophisticated technologies, such as magnetic recording, storage and reading devices [5–11].

Theoretically, such systems have been studied by several statistical mechanical methods: renormalization-group technique [12, 13], mean-field approximation [14–18], effective-field theory [19–24], Monte Carlo simulations [25–29]. Recently, Jiang and Bai [30] have studied the influence of an external longitudinal magnetic field on the magnetic properties of a mixed spin-1/2 and spin-3/2 Ising ferromagnetic/ferrimagnetic bilayer system. By means of the effective-field theory, Essaoudi et al. [31] also studied the same model using a probability distribution technique. This investigation revealed a remarkable influence of the field strength on the magnetic properties of this system. Few exactly solved mixed-Ising models exist in the literature. For recent review on the subject, the reader should refer to references [32–41]. Experimentally, the investigation of such systems has been performed for many years and has shown strong effects of the external constraint on the physical properties of the system [42, 43].

*fhontinfinde@yahoo.fr

In this paper, the Bethe lattice (BL) approach is used to examine the magnetic properties of the mixed spin- $\frac{1}{2}$ and spin- $\frac{7}{2}$ Ising model with equal crystal-field in the presence of a longitudinal magnetic field. The exact recursion relations are calculated considering contribution to the total partition function of the system from sites deep inside the lattice [44]. This work aims at the study of the effects on the phase boundaries of the competition between the two parameters of the system: the magnetic field and the crystal-field strengths.

The remainder of this paper is arranged as follows. In section 2, the formulation of the model on the BL is clarified. Also, the order-parameters, the corresponding response functions, the internal energy and free energy are expressed in terms of recursion relations. In section 3, we discuss in detail the numerical results. Finally, in the last section we conclude.

2. Formulation of the model on the BL

The mixed-spin system on the BL is shown in figure 1. It consists of two sublattices A and B. Sites of the sublattice A are occupied by atoms of spins $s_i = \pm\frac{1}{2}$. Those of the sublattice B are occupied by atoms of spins $\sigma_j = \pm\frac{7}{2}, \pm\frac{5}{2}, \pm\frac{3}{2}, \pm\frac{1}{2}$. The BL is arranged such that the central spin is spin- $\frac{1}{2}$, and the next generation spin is spin- $\frac{7}{2}$ and so on to infinity. The Ising Hamiltonian of the model may be written as:

$$H = -J \sum_{\langle i,j \rangle} s_i \sigma_j - D \sum_j \sigma_j^2 - h \left(\sum_i s_i + \sum_j \sigma_j \right), \quad (1)$$

where $J < 0$ is the bilinear exchange coupling interaction strength; D and h are, respectively, the crystal-field and the longitudinal magnetic field acting on the spins.

In order to formulate the problem on the BL, the partition function is calculated. Its expression reads:

$$Z = \sum \exp \left\{ \beta \left[J \sum_{\langle i,j \rangle} s_i \sigma_j + D \sum_j \sigma_j^2 + h \left(\sum_i s_i + \sum_j \sigma_j \right) \right] \right\}. \quad (2)$$

If the BL is cut at the central spin s_0 , it splits into z disconnected pieces. Then, the partition function can be written as:

$$Z = \sum_{s_0} \exp [\beta(hs_0)] g_n^z(s_0), \quad (3)$$

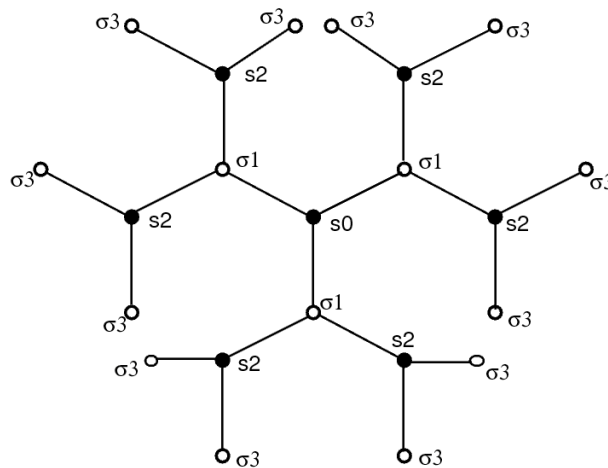


Figure 1. Schematic representation of the Bethe lattice with coordination number $z = 3$. It consists of two interpenetrating sublattices A and B with spin variables $s_i = 1/2$ and $\sigma_j = 7/2$, respectively.

where s_0 is the central spin value of the lattice, $g_n(s_0)$ is the partition function of an individual branch and the suffix n represents the fact that the sub-tree has n shells, i.e., n steps from the root to the boundary sites. If one continues to cut the BL on spins σ_1 and s_2 which are respectively the nearest and next-nearest neighbors of the central spin s_0 , the recurrence relations for $g_n(s_0)$ and $g_{n-1}(\sigma_1)$ read:

$$g_n(s_0) = \sum_{\{\sigma_1\}} \exp [\beta(Js_0\sigma_1 + D\sigma_1^2 + h\sigma_1)] [g_{n-1}(\sigma_1)]^{z-1}, \quad (4)$$

$$g_{n-1}(\sigma_1) = \sum_{\{s_2\}} \exp [\beta(Js_2\sigma_1 + hs_2)] [g_{n-2}(s_2)]^{z-1}. \quad (5)$$

Explicit relations for some $g_n(s_0)$ and $g_{n-1}(\sigma_1)$ are given in the following:

$$\begin{aligned} g_n\left(\pm\frac{1}{2}\right) &= \sum_{\{\sigma_1\}} \exp \left[\beta \left(\pm \frac{J}{2}\sigma_1 + D\sigma_1^2 + h\sigma_1 \right) \right] [g_{n-1}(\sigma_1)]^{z-1} \\ &= \exp \left[\beta \left(\pm \frac{7J}{4} + \frac{49}{4}D + \frac{7}{2}h \right) \right] \left[g_{n-1}\left(\frac{7}{2}\right) \right]^{z-1} \\ &+ \exp \left[\beta \left(\mp \frac{7J}{4} + \frac{49}{4}D - \frac{7}{2}h \right) \right] \left[g_{n-1}\left(-\frac{7}{2}\right) \right]^{z-1} \\ &+ \exp \left[\beta \left(\pm \frac{5J}{4} + \frac{25}{4}D + \frac{5}{2}h \right) \right] \left[g_{n-1}\left(\frac{5}{2}\right) \right]^{z-1} \\ &+ \exp \left[\beta \left(\mp \frac{5J}{4} + \frac{25}{4}D - \frac{5}{2}h \right) \right] \left[g_{n-1}\left(-\frac{5}{2}\right) \right]^{z-1} \\ &+ \exp \left[\beta \left(\pm \frac{3J}{4} + \frac{9}{4}D + \frac{3}{2}h \right) \right] \left[g_{n-1}\left(\frac{3}{2}\right) \right]^{z-1} \\ &+ \exp \left[\beta \left(\mp \frac{3J}{4} + \frac{9}{4}D - \frac{3}{2}h \right) \right] \left[g_{n-1}\left(-\frac{3}{2}\right) \right]^{z-1} \\ &+ \exp \left[\beta \left(\pm \frac{J}{4} + \frac{1}{4}D + \frac{1}{2}h \right) \right] \left[g_{n-1}\left(\frac{1}{2}\right) \right]^{z-1} \\ &+ \exp \left[\beta \left(\mp \frac{J}{4} + \frac{1}{4}D - \frac{1}{2}h \right) \right] \left[g_{n-1}\left(-\frac{1}{2}\right) \right]^{z-1}, \end{aligned} \quad (6)$$

$$\begin{aligned} g_{n-1}\left(\pm\frac{7}{2}\right) &= \sum_{\{s_2\}} \exp \left[\beta \left(\pm \frac{7J}{2}s_2 + hs_2 \right) \right] [g_{n-2}(s_2)]^{z-1} \\ &= \exp \left[\beta \left(\pm \frac{7J}{4} + \frac{h}{2} \right) \right] \left[g_{n-2}\left(\frac{1}{2}\right) \right]^{z-1} \\ &+ \exp \left[\beta \left(\mp \frac{7J}{4} - \frac{h}{2} \right) \right] \left[g_{n-2}\left(-\frac{1}{2}\right) \right]^{z-1}, \end{aligned} \quad (7)$$

$$\begin{aligned} g_{n-1}\left(\pm\frac{5}{2}\right) &= \sum_{\{s_2\}} \exp \left[\beta \left(\pm \frac{5J}{2}s_2 + hs_2 \right) \right] [g_{n-2}(s_2)]^{z-1} \\ &= \exp \left[\beta \left(\pm \frac{5J}{4} + \frac{h}{2} \right) \right] \left[g_{n-2}\left(\frac{1}{2}\right) \right]^{z-1} \\ &+ \exp \left[\beta \left(\mp \frac{5J}{4} - \frac{h}{2} \right) \right] \left[g_{n-2}\left(-\frac{1}{2}\right) \right]^{z-1}, \end{aligned} \quad (8)$$

$$\begin{aligned}
g_{n-1}\left(\pm\frac{3}{2}\right) &= \sum_{\{s_2\}} \exp\left[\beta\left(\pm\frac{3J}{2}s_2 + hs_2\right)\right] [g_{n-2}(s_2)]^{z-1} \\
&= \exp\left[\beta\left(\pm\frac{3J}{4} + \frac{h}{2}\right)\right] \left[g_{n-2}\left(\frac{1}{2}\right)\right]^{z-1} \\
&+ \exp\left[\beta\left(\mp\frac{3J}{4} - \frac{h}{2}\right)\right] \left[g_{n-2}\left(-\frac{1}{2}\right)\right]^{z-1}, \tag{9}
\end{aligned}$$

$$\begin{aligned}
g_{n-1}\left(\pm\frac{1}{2}\right) &= \sum_{\{s_2\}} \exp\left[\beta\left(\pm\frac{1J}{2}s_2 + hs_2\right)\right] [g_{n-2}(s_2)]^{z-1} \\
&= \exp\left[\beta\left(\pm\frac{1J}{4} + \frac{h}{2}\right)\right] \left[g_{n-2}\left(\frac{1}{2}\right)\right]^{z-1} \\
&+ \exp\left[\beta\left(\mp\frac{1J}{4} - \frac{h}{2}\right)\right] \left[g_{n-2}\left(-\frac{1}{2}\right)\right]^{z-1}. \tag{10}
\end{aligned}$$

After calculating all the $g_n(s_0)$ and $g_{n-1}(\sigma_1)$, the recursion relations for the spin- $\frac{1}{2}$ are defined as:

$$Y_n = \frac{g_n\left(\frac{1}{2}\right)}{g_n\left(-\frac{1}{2}\right)} \tag{11}$$

and for the spin- $\frac{7}{2}$ as:

$$A_{n-1} = \frac{g_{n-1}\left(+\frac{7}{2}\right)}{g_{n-1}\left(-\frac{1}{2}\right)}, \quad B_{n-1} = \frac{g_{n-1}\left(-\frac{7}{2}\right)}{g_{n-1}\left(-\frac{1}{2}\right)}, \tag{12}$$

$$C_{n-1} = \frac{g_{n-1}\left(+\frac{5}{2}\right)}{g_{n-1}\left(-\frac{1}{2}\right)}, \quad D_{n-1} = \frac{g_{n-1}\left(-\frac{5}{2}\right)}{g_{n-1}\left(-\frac{1}{2}\right)}, \tag{13}$$

$$E_{n-1} = \frac{g_{n-1}\left(\frac{3}{2}\right)}{g_{n-1}\left(-\frac{1}{2}\right)}, \quad F_{n-1} = \frac{g_{n-1}\left(-\frac{3}{2}\right)}{g_{n-1}\left(-\frac{1}{2}\right)},$$

$$G_{n-1} = \frac{g_{n-1}\left(+\frac{1}{2}\right)}{g_{n-1}\left(-\frac{1}{2}\right)}.$$

For the numerical investigation of the model, the magnetization M and the corresponding quadrupolar moment Q are quantities of interest. For the sublattice A, the sublattice magnetization $M_{1/2}$ is defined by:

$$M_{1/2} = Z_{1/2}^{-1} \sum_{\{s_0\}} s_0 \exp(\beta h s_0) g_n^z(s_0). \tag{14}$$

After some mathematical manipulations, the sublattice magnetization $M_{1/2}$ is explicitly given by:

$$M_{1/2} = \frac{\exp\left(\frac{\beta h}{2}\right) Y_n^z - \exp\left(-\frac{\beta h}{2}\right)}{2\left[\exp\left(\frac{\beta h}{2}\right) Y_n^z + \exp\left(-\frac{\beta h}{2}\right)\right]}. \tag{15}$$

In the same way, the two order-parameters for the sublattice B are calculated as follows:

$$M_{7/2} = \frac{M'_{7/2}}{M^0_{7/2}}, \quad Q_{7/2} = \frac{Q'_{7/2}}{Q^0_{7/2}}, \tag{16}$$

where

$$\begin{aligned}
 M'_{7/2} &= 7 \exp\left(\frac{49}{4}\beta D\right) \left[\exp\left(\frac{7}{2}\beta h\right) A_{n-1}^z - \exp\left(-\frac{7}{2}\beta h\right) B_{n-1}^z \right] \\
 &+ 5 \exp\left(\frac{25}{4}\beta D\right) \left[\exp\left(\frac{5}{2}\beta h\right) C_{n-1}^z - \exp\left(-\frac{5}{2}\beta h\right) D_{n-1}^z \right] \\
 &+ 3 \exp\left(\frac{9}{4}\beta D\right) \left[\exp\left(\frac{3}{2}\beta h\right) E_{n-1}^z - \exp\left(-\frac{3}{2}\beta h\right) F_{n-1}^z \right] \\
 &+ \exp\left(\frac{1}{4}\beta D\right) \left[\exp\left(\frac{1}{2}\beta h\right) G_{n-1}^z - \exp\left(-\frac{1}{2}\beta h\right) \right], \tag{17}
 \end{aligned}$$

$$\begin{aligned}
 M_{7/2}^0 &= 2 \exp\left(\frac{49}{4}\beta D\right) \left[\exp\left(\frac{7}{2}\beta h\right) A_{n-1}^z + \exp\left(-\frac{7}{2}\beta h\right) B_{n-1}^z \right] \\
 &+ 2 \exp\left(\frac{25}{4}\beta D\right) \left[\exp\left(\frac{5}{2}\beta h\right) C_{n-1}^z + \exp\left(-\frac{5}{2}\beta h\right) D_{n-1}^z \right] \\
 &+ 2 \exp\left(\frac{9}{4}\beta D\right) \left[\exp\left(\frac{3}{2}\beta h\right) E_{n-1}^z + \exp\left(-\frac{3}{2}\beta h\right) F_{n-1}^z \right] \\
 &+ 2 \exp\left(\frac{1}{4}\beta D\right) \left[\exp\left(\frac{1}{2}\beta h\right) G_{n-1}^z + \exp\left(-\frac{1}{2}\beta h\right) \right], \tag{18}
 \end{aligned}$$

$$\begin{aligned}
 Q'_{7/2} &= 49 \exp\left(\frac{49}{4}\beta D\right) \left[\exp\left(\frac{7}{2}\beta h\right) A_{n-1}^z + \exp\left(-\frac{7}{2}\beta h\right) B_{n-1}^z \right] \\
 &+ 25 \exp\left(\frac{25}{4}\beta D\right) \left[\exp\left(\frac{5}{2}\beta h\right) C_{n-1}^z + \exp\left(-\frac{5}{2}\beta h\right) D_{n-1}^z \right] \\
 &+ 9 \exp\left(\frac{9}{4}\beta D\right) \left[\exp\left(\frac{3}{2}\beta h\right) E_{n-1}^z + \exp\left(-\frac{3}{2}\beta h\right) F_{n-1}^z \right] \\
 &+ \exp\left(\frac{1}{4}\beta D\right) \left[\exp\left(\frac{1}{2}\beta h\right) G_{n-1}^z + \exp\left(-\frac{1}{2}\beta h\right) \right], \tag{19}
 \end{aligned}$$

$$\begin{aligned}
 Q_{7/2}^0 &= 4 \exp\left(\frac{49}{4}\beta D\right) \left[\exp\left(\frac{7}{2}\beta h\right) A_{n-1}^z + \exp\left(-\frac{7}{2}\beta h\right) B_{n-1}^z \right] \\
 &= 4 \exp\left(\frac{25}{4}\beta D\right) \left[\exp\left(\frac{5}{2}\beta h\right) C_{n-1}^z + \exp\left(-\frac{5}{2}\beta h\right) D_{n-1}^z \right] \\
 &+ 4 \exp\left(\frac{9}{4}\beta D\right) \left[\exp\left(\frac{3}{2}\beta h\right) E_{n-1}^z + \exp\left(-\frac{3}{2}\beta h\right) F_{n-1}^z \right] \\
 &+ 4 \exp\left(\frac{1}{4}\beta D\right) \left[\exp\left(\frac{1}{2}\beta h\right) G_{n-1}^z + \exp\left(-\frac{1}{2}\beta h\right) \right]. \tag{20}
 \end{aligned}$$

In order to determine the compensation temperature, one should define the global magnetization M_{net} of the model which is given by:

$$M_{\text{net}} = \frac{M_{1/2} + M_{7/2}}{2}. \tag{21}$$

To really study the model in detail and single out the influence of the crystal-field and the applied magnetic field on the magnetic properties of the model, we have also examined the thermal variations of the response functions i.e., the susceptibilities, the specific heat and the internal energy defined respectively by:

$$\chi_{\text{Total}} = \chi_{1/2} + \chi_{7/2} = \left(\frac{\partial M_{1/2}}{\partial h} \right)_{h=0} + \left(\frac{\partial M_{7/2}}{\partial h} \right)_{h=0}, \tag{22}$$

$$C = -\beta^2 \frac{\partial^2(-\beta F')}{\partial \beta^2}, \quad (23)$$

$$\frac{U}{N|J|} = -k_B T^2 \frac{\partial}{\partial T} \left(\frac{F'}{k_B T} \right), \quad (24)$$

where F' is the free energy of the model.

In order to classify the order of the phase transitions, i.e., whether the second- or the first-order, the free energy expression is also needed in addition to the order-parameters. It can be calculated in terms of recurrence relations by using the definition $F' = -kT \ln(Z)$ in the thermodynamic limit, i.e., $n \rightarrow \infty$:

$$\begin{aligned} \frac{F'}{J} = & -\frac{1}{\beta'} \left(\frac{z-1}{2-z} \ln \left\{ \exp \left[\beta \left(-\frac{J}{4} + \frac{h}{2} \right) \right] Y_n^{z-1} + \exp \left[\beta \left(\frac{J}{4} - \frac{h}{2} \right) \right] \right\} \right) \\ & - \frac{1}{\beta'} \left(\ln \left\{ \exp \left[\beta \left(\frac{h}{2} \right) \right] Y_n^z + \exp \left[\beta \left(-\frac{h}{2} \right) \right] \right\} \right) \\ & - \frac{1}{\beta'} \left(\frac{1}{2-z} \ln \left\{ \exp \left[\beta \left(-\frac{7J}{4} + \frac{49D}{4} + \frac{7h}{2} \right) \right] A_{n-1}^{z-1} \right. \right. \\ & + \exp \left[\beta \left(\frac{7J}{4} + \frac{49D}{4} - \frac{7h}{2} \right) \right] B_{n-1}^{z-1} \\ & + \exp \left[\beta \left(-\frac{5J}{4} + \frac{25D}{4} + \frac{5h}{2} \right) \right] C_{n-1}^{z-1} + \exp \left[\beta \left(\frac{5J}{4} + \frac{25D}{4} - \frac{5h}{2} \right) \right] D_{n-1}^{z-1} \\ & + \exp \left[\beta \left(-\frac{3J}{4} + \frac{9D}{4} + \frac{3h}{2} \right) \right] E_{n-1}^{z-1} + \exp \left[\beta \left(\frac{3J}{4} + \frac{9D}{4} - \frac{3h}{2} \right) \right] F_{n-1}^{z-1} \\ & \left. \left. + \exp \left[\beta \left(-\frac{J}{4} + \frac{D}{4} + \frac{h}{2} \right) \right] G_{n-1}^{z-1} + \exp \left[\beta \left(\frac{J}{4} + \frac{D}{4} - \frac{h}{2} \right) \right] \right\} \right). \quad (25) \end{aligned}$$

3. Numerical results and discussions

In this section, we present and discuss the results we obtained for the temperature phase diagrams of the model, the thermal variations of the order-parameters, the response functions and the internal energy. To this end, we first construct the phase diagram at $T = 0$.

3.1. Ground-state phase diagrams

The ground-state phase diagram of the model is obtained by comparing the values of the energy E_0 for different spin configurations which can be expressed as:

$$E_0 = s\sigma - \frac{1}{z|J|} [D\sigma^2 + h(s + \sigma)]. \quad (26)$$

Only eight possible pairs of spins due to the ferrimagnetic coupling J and positive field ($h \geq 0$) are found. Calculations of these energies in the $(h/z|J|, D/z|J|)$ plane yield the ground-state phase diagram displayed in figure 2. The model has a usual spin-flip symmetry. Thus, all ground-states for negative field ($h < 0$) can be obtained from the corresponding ones at a positive field, simply by reversing all spin orientations. Some key features of the model are revealed in the diagram, in particular, the existence of seven multicritical points (A_1, A_2, \dots, A_7) and coexistence lines where spin pair energies of some phases are equal. In the absence of the magnetic field, for a given values of z and $D/z|J|$, $M_{7/2}$ shows seven saturation values whereas for $M_{1/2}$, $\pm \frac{1}{2}$ are the two saturation values. Hence, we get the ferrimagnetic phases: $\mathbf{F}(\mp \frac{1}{2}, \pm \frac{7}{2})$, $\mathbf{F}(\mp \frac{1}{2}, \pm \frac{5}{2})$, $\mathbf{F}(\mp \frac{1}{2}, \pm \frac{3}{2})$, $\mathbf{F}(\mp \frac{1}{2}, \pm \frac{1}{2})$ and at the borders of these phases, three hybrid

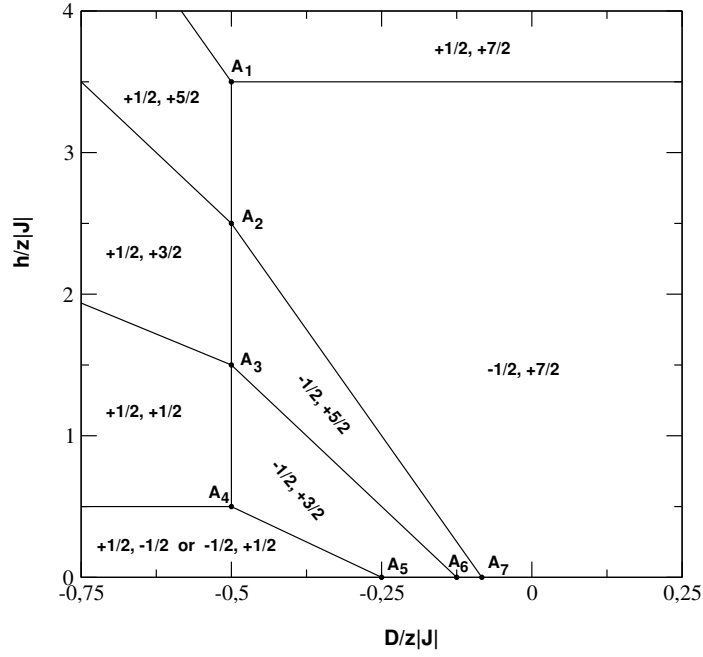


Figure 2. Ground-state phase diagram of the mixed spin- $\frac{1}{2}$ and spin- $\frac{7}{2}$ Ising ferrimagnetic model with the crystal-field D applied one sublattice in the $(h/z|J|, D/z|J|)$ plane. There exist eight stable phases. Along the $D/z|J|$ -axis and for all values of z , three hybrid phases may appear at the multicritical points A_5 , A_6 and A_7 .

phases: $\mathbf{F}(\mp \frac{1}{2}, \pm 1)$, $\mathbf{F}(\mp \frac{1}{2}, \pm 2)$, $\mathbf{F}(\mp \frac{1}{2}, \pm 3)$ at the multicritical points A_5 , A_6 and A_7 , respectively. These hybrid phases should correspond to cases where the sublattice B is half-half covered by spins of the two neighboring phases.

3.2. Finite-temperature phase diagrams

In this subsection, we show some typical results for the mixed spin- $\frac{1}{2}$ and spin- $\frac{7}{2}$ Ising model on the BL with a crystal field at zero longitudinal magnetic field. First, we present phase diagrams of the model in the $(D/|J|, k_B T/|J|)$ plane for $z = 3, 4$ and 6 . Therein, solid lines indicate a second-order transition. The three filled circles A_5 , A_6 and A_7 in figure 3 are the multicritical points found in the ground-state phase diagram.

From this figure, some interesting properties of the system emerge. Indeed, for all values of the coordination number z , from panel (a) to panel (c), transition lines are only of the second-order type and separate the ferrimagnetic phase (\mathbf{F}) which is a mixture of five different ferrimagnetic phases from the paramagnetic phase (P). They become constant for $D/|J| < -\frac{z}{12}$. One observes that for $D/|J| > -\frac{z}{12}$, the second-order phase transition turns from ferrimagnetic phase $\mathbf{F}(\mp \frac{1}{2}, \pm \frac{7}{2})$ to the disordered paramagnetic phase P . For $-\frac{z}{8} < D/|J| < -\frac{z}{12}$, the second-order phase transition is from the ferrimagnetic $\mathbf{F}(\mp \frac{1}{2}, \pm \frac{5}{2})$ to the paramagnetic phase P . When $-\frac{z}{4} < D/|J| < -\frac{z}{8}$, the second-order phase transition is from the ferrimagnetic $\mathbf{F}(\mp \frac{1}{2}, \pm \frac{3}{2})$ to the paramagnetic phase P . In the case where $D/|J| < -\frac{z}{4}$, the second-order phase transition is from the ferrimagnetic phase $\mathbf{F}(\pm \frac{1}{2}, \mp \frac{1}{2})$ to the paramagnetic phase P . For $D/|J| = -\frac{z}{12}$, (respectively $D/|J| = -\frac{z}{8}$ and $D/|J| = -\frac{z}{4}$), the second-order transition phase is from the hybrid phase $\mathbf{F}(\mp \frac{1}{2}, \pm 3)$ [respectively the hybrid phase $\mathbf{F}(\mp \frac{1}{2}, \pm 2)$ and $\mathbf{F}(\mp \frac{1}{2}, \pm 1)$] to the paramagnetic phase P .

It is important to mention that figure 3 presents some resemblances with results from references [24, 36, 40] concerning the second-order transition lines. Also, by increasing the value of the coordination number z , the ferrimagnetic domain \mathbf{F} becomes important.

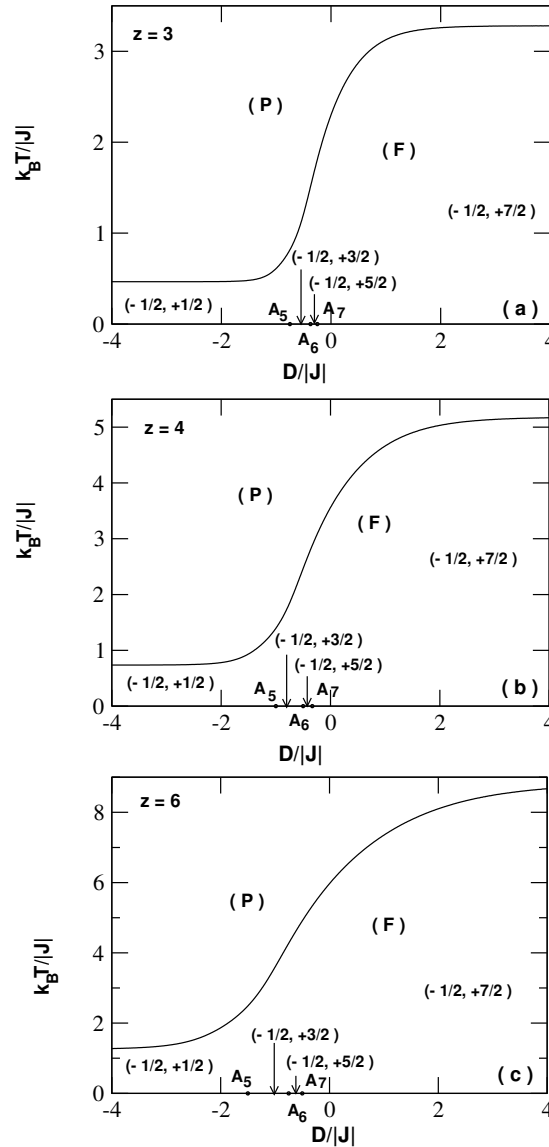


Figure 3. Phase diagrams of the model in the $(D/|J|, k_B T/|J|)$ plane. The black circles on the $D/|J|$ -axis correspond to the A_5 , A_6 and A_7 multicritical points obtained in the ground-state phase diagram and the solid line indicates the second-order transition line. Panel (a): $z = 3$; panel (b): $z = 4$ and panel (c): $z = 6$. Here, the model only presents second-order transition for all values of z . The multicritical points A_5 , A_6 and A_7 which respectively indicate the positions of the hybrid phases $F(\mp \frac{1}{2}, \pm 3)$, $F(\mp \frac{1}{2}, \pm 2)$, and $F(\mp \frac{1}{2}, \pm 1)$ respectively, separate the ferrimagnetic phases $F(\mp \frac{1}{2}, \pm \frac{7}{2})$, $F(\mp \frac{1}{2}, \pm \frac{5}{2})$, $F(\mp \frac{1}{2}, \pm \frac{3}{2})$, and $F(\mp \frac{1}{2}, \pm \frac{1}{2})$.

3.3. Thermal variations of the order-parameters, the response functions and the internal energy

As it is explained above, the thermal variations of the order-parameters, the response functions and the internal energy for the model were calculated in terms of recursion relations. The thermal variations of the order-parameters are crucial for obtaining the temperature dependence phase diagrams of the model. In fact, when the magnetization curves go to zero continuously, one gets a second-order phase transition. In the case of a jump in the magnetizations curves followed by a discontinuity of the first derivative of the free-energy F' , a first-order transition temperature is got. Besides these two temperatures, there is another

temperature called compensation temperature defined as the temperature where the global magnetization becomes zero before the critical temperature. Therefore, in order to identify transition and compensation lines, one needs to study the thermal behaviours of the considered thermodynamical quantities of the model. Now, we present some results on the thermal behaviours of the order-parameters, the response functions and the internal energy in the absence of the magnetic field h when $z = 3, 4$ and 6 .

Figure 4 illustrates some thermal variations of the sublattice magnetizations $M_{1/2}$ and $M_{7/2}$ when $z = 3, 4$ and 6 for selected values of the crystal-field $D/|J|$. The results are in perfect agreement with the ground-state phase diagram concerning the saturation values. Indeed, $M_{1/2}$ falls from its unique saturation value $\mp \frac{1}{2}$ with an increasing temperature whereas $M_{7/2}$ shows seven saturation values. The behaviours of the sublattice magnetizations $M_{1/2}$ and $M_{7/2}$ are quite similar. Moreover, one can notice

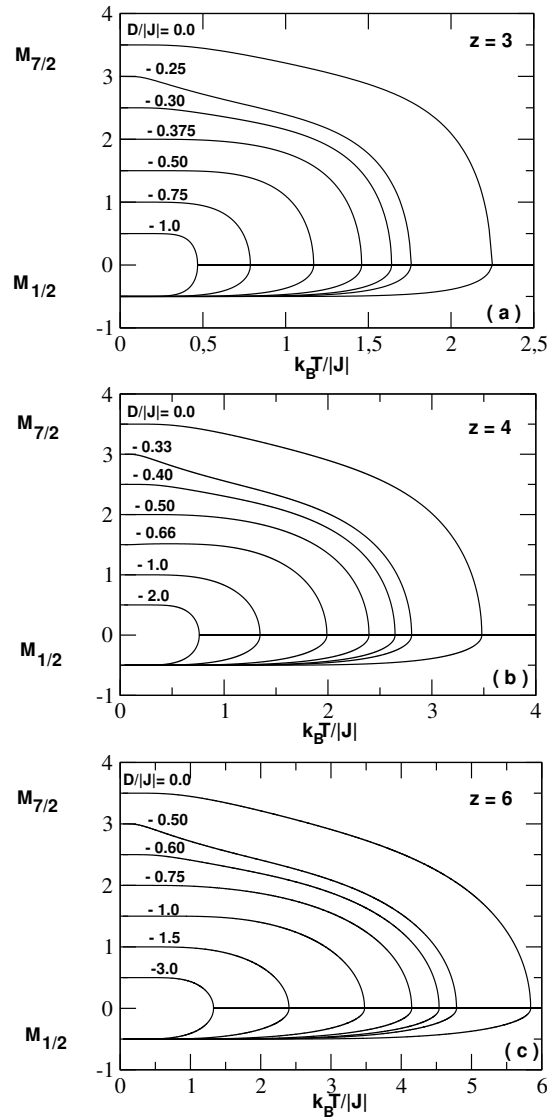


Figure 4. Sublattice magnetizations of the model as functions of the reduced temperature $k_B T / |J|$ for $z = 3, 4$ and 6 for various values of the crystal-field interactions D . Panel (a): curves are displayed for $z = 3$ and selected values of $D/|J|$ are indicated on the curves. Panel (b): curves are displayed for $z = 4$ and selected values of $D/|J|$ indicated on the curves. Panel (c): curves are displayed for $z = 6$ and selected values of $D/|J|$ indicated on the curves. For all values of z , the sublattice magnetization curves are all continuous.

that all the curves are continuous and the Curie temperature T_c at which both magnetization curves go to zero increases with the crystal-field $D/|J|$ and the coordination number z .

In figure 5, we have plotted the thermal variations of the specific heat and the internal energy for various values of the crystal-field as indicated in the figure. Both the specific heat and the internal energy rapidly increase with increasing temperature and make peak without jump discontinuities at the same T_c . By increasing the strength of the crystal-field and the coordination number, the value of T_c at which the transition occurs, increases and this can be easily observed by comparing the results from different panels of figure 5. The results obtained in this figure confirm that the model only presents second-order transition for all values of the coordination number z .

In figure 6, we also present the temperature dependences of both sublattice magnetizations and susceptibilities when $z = 3, 4, 6$ and $D/|J| = 1$. From this figure, the value of the transition temperature T_c increases with an increasing coordination number z . Here, T_c separates the ferrimagnetic phase $F(\pm \frac{1}{2}, \mp \frac{7}{2})$ from the paramagnetic phase (P) and $T_c/|J| = 3.110$ (respectively $T_c/|J| = 4.644$ and 7.313) for $z = 3$ (respectively for $z = 4$ and 6). Furthermore, one remarks that for $T \rightarrow T_c$, $\chi_{7/2} \rightarrow +\infty$ whereas $\chi_{1/2} \rightarrow -\infty$. For $T > T_c$, the susceptibility $\chi_{1/2}$ rapidly increases whereas the susceptibility $\chi_{7/2}$ rapidly decreases when the temperature increases and is very far from the Curie temperature T_c , $\chi_{7/2} \rightarrow 0$ and $\chi_{1/2} \rightarrow 0$.

Let us now discuss the thermal variations of the sublattice magnetizations, the corresponding response functions and the internal energy of the system in the presence of the longitudinal magnetic field h .

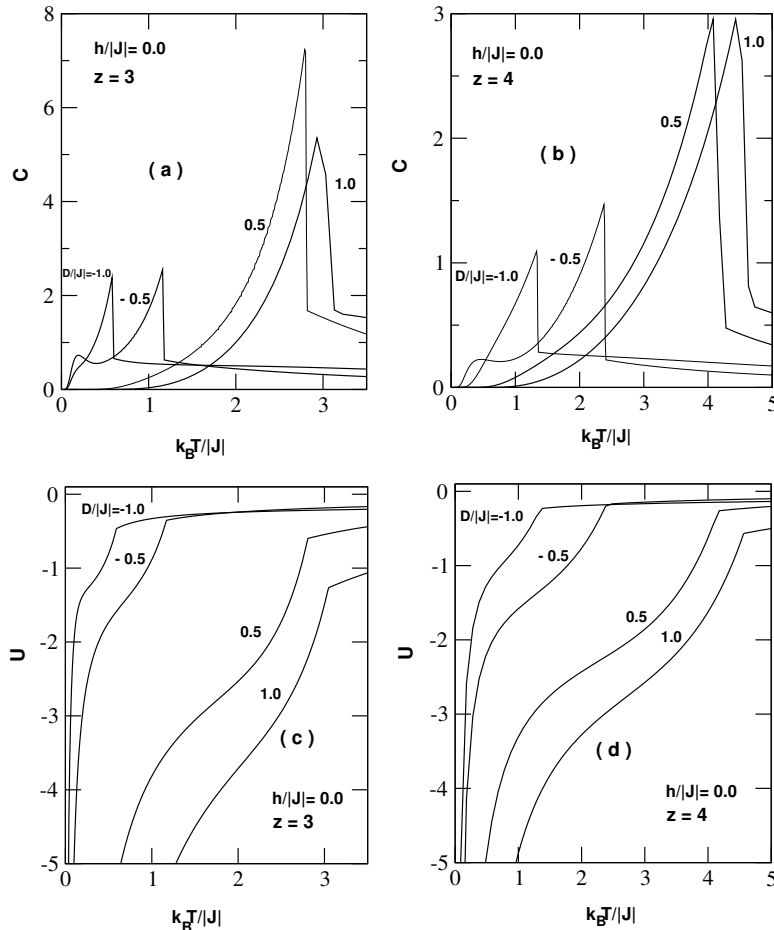


Figure 5. Thermal variations of the specific heat and internal energy are calculated for $z = 3, 4$ and selected values of the crystal-field $D/|J|$ as shown in the figures from panel (a) to panel (d). Values of the physical parameters considered are indicated in different panels. Analysis of the data in different panels shows that the model only exhibits second-order transition for $z = 3, 4$.

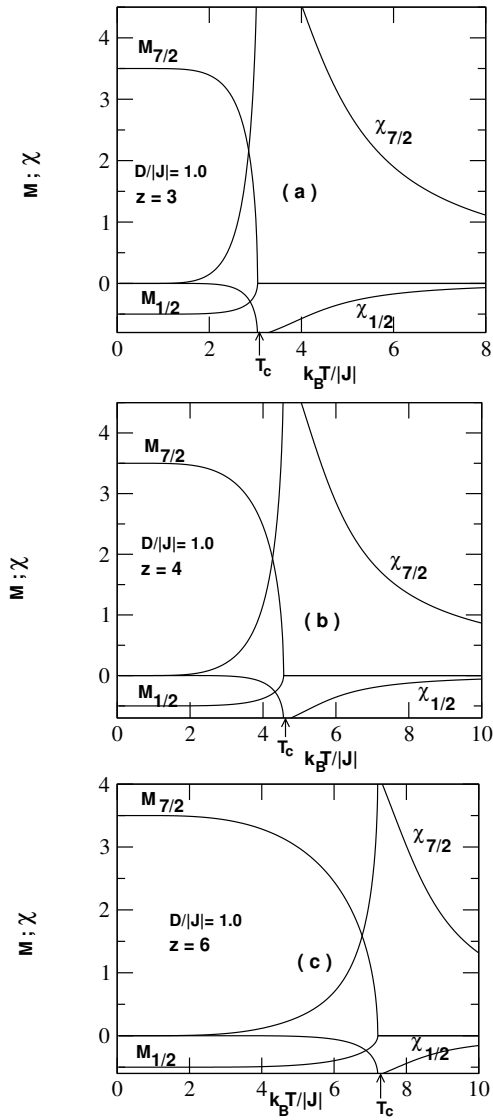


Figure 6. The behaviour of the sublattice magnetizations and magnetic susceptibilities as a function of temperature on the Bethe lattice for $z = 3, 4$ and 6 when $D/|J| = 1.0$. Values of the physical parameters considered for the system are indicated in different panels.

Figure 7 expresses the effects of an applied magnetic field h on the magnetic properties of the model when $z = 3$ and $D/|J| = 1.0$ for selected values of $h/|J|$. In panel (a), the sublattice magnetizations continuously decrease from their saturation values to non-zero values when the temperature increases. The remaining values of the sublattice magnetizations are more important when the value of the applied magnetic field is high. Thus, one observes that the system does not present any transition when $h/|J| \neq 0$. It is important to indicate that in the case of $h/|J| = 0$, the model exhibits the second-order transition at a Curie temperature $T_c/|J| = 3.110$, where the two sublattice magnetizations continuously go to zero after decreasing from their saturation values at $T = 0$. In panels (b), (c) and (d), we have displayed the temperature dependence of the total susceptibility χ_T , the internal energy U and the specific heat C , respectively. One can see from these panels that the response functions and the internal energy indicate a second-order transition which occurs at the same $T_c/|J|$ as in the case of $h/|J| = 0$. For $h/|J| \neq 0$ and $T > T_c$, the response functions exhibit a maximum and the height of the maximum decreases when the value of the applied magnetic field increases.

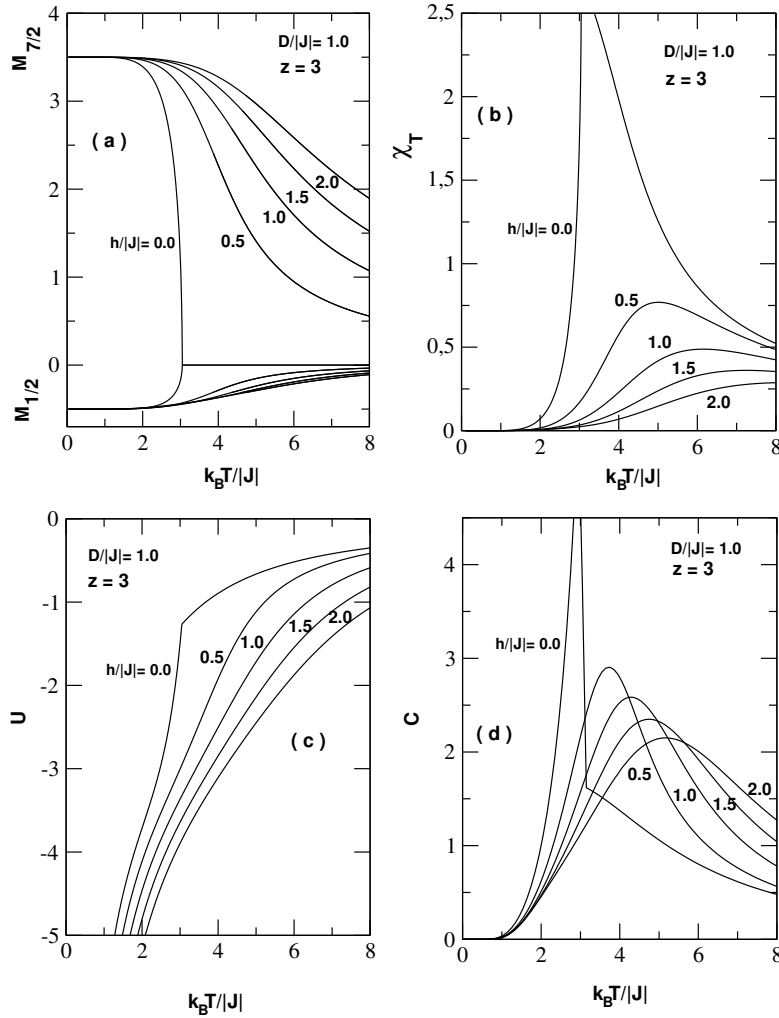


Figure 7. The temperature dependence of the sublattice magnetizations $M_{1/2}$, $M_{7/2}$ [panel (a)], the total susceptibility χ_T [panel (b)], the total internal energy U [panel (c)] and the total specific heat C [panel (d)]. The following values of the parameters are used: $D/|J| = 1.0$; $h/|J| = 0.0; 0.5; 1.0; 1.5; 2.0$.

In figure 8, we have presented the thermal variations of the response functions for some values of the system parameters to show the influence of $D/|J|$ on the system properties for $h/|J| \neq 0$. In the figure, one observes that the response functions show interesting behaviours. Indeed, the two studied response functions globally show a maximum at a certain value of the temperature. This temperature increases with the coordination number and the strength of the crystal-field. It is important to mention that the height of the maximum of the two response functions also increases with increasing values of the strength of the crystal-field $D/|J|$ but the opposite holds when the coordination number z increases.

In figure 9, we have investigated the global magnetization as a function of the temperature and obtained some compensation types of the model. The figure shows temperature dependencies of the global magnetization M_{net} for selected values of the crystal-field when $z = 3$. As seen from figure 9, the model exhibits five types of compensation behaviours, namely R-, S-, P-, Q- and L-type compensation behaviours as classified in the extended Néel nomenclature [45–48].

Moreover, we investigate the low-temperature magnetic properties of the model. We plotted the sublattice magnetizations and the global magnetization at $k_B T/|J| = 0.1$ for selected values of the crystal-field as functions of the field h as shown in figure 10. In panel (a) where $D/|J| = -1$ and $z = 3$, M_{net} and $M_{7/2}$ respectively show five and four step-like magnetization plateaus ($M_{\text{net}} = 0, \frac{1}{2}, 1, \frac{3}{2}, 2$) and ($M_{7/2} = \frac{1}{2}, \frac{3}{2}, \frac{5}{2}, \frac{7}{2}$) whereas $M_{1/2}$ shows two step-like magnetization plateaus ($M_{1/2} = -\frac{1}{2}, \frac{1}{2}$). Also, from

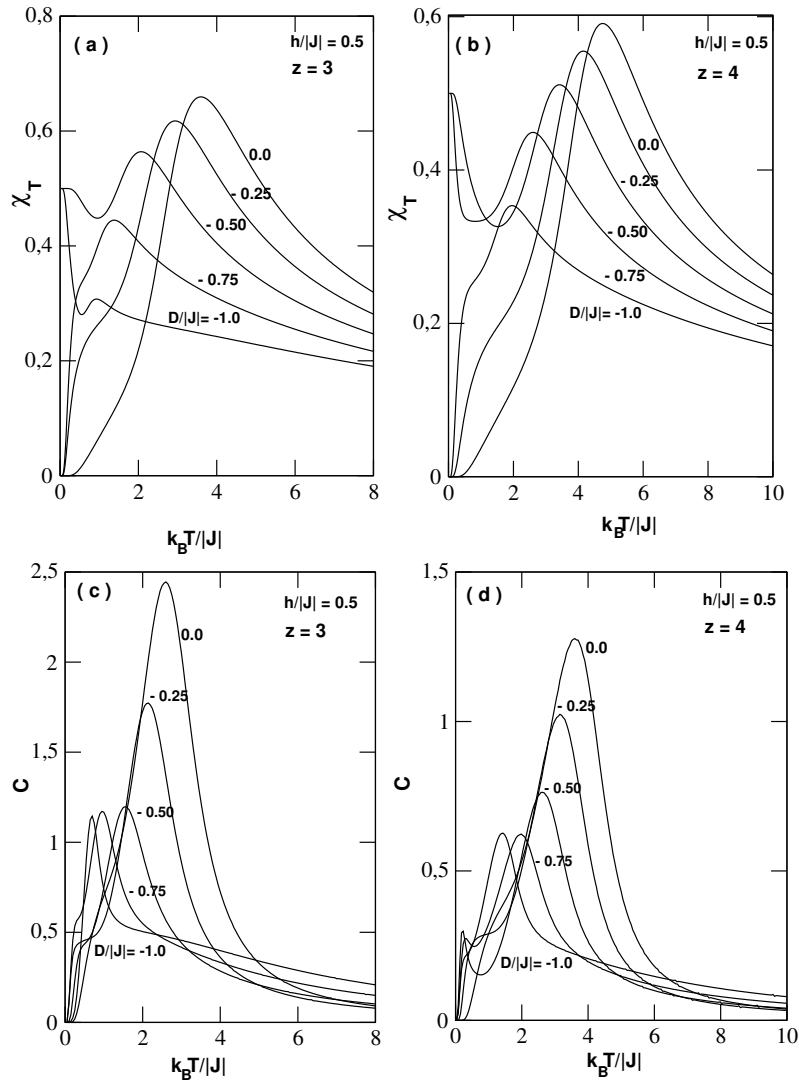


Figure 8. Temperature variations of the response functions of the model at selected values of $D/|J|$ indicated on different curves illustrated for $z = 3, 4$ and $h/|J| = 0.5$.

panel (b) where $D/|J| = 0$ and $z = 3$, only M_{net} and $M_{1/2}$ present two step-like magnetization plateaus ($M_{\text{net}} = \frac{3}{2}, 2$) and ($M_{1/2} = -\frac{1}{2}, \frac{1}{2}$). These obtained results are consistent with the ground-state phase diagram displayed in figure 2 of references [49, 50].

4. Conclusion

In this paper, we have studied the magnetic properties of the mixed spin- $\frac{1}{2}$ and spin- $\frac{7}{2}$ Ising ferrimagnetic model on the BL in the presence of a longitudinal magnetic field by means of the recursion relations method. All the thermodynamical quantities of interest are calculated as functions of recursion relations.

The ground-state phase diagram of the model is displayed as shown in figure 2. From this phase diagram, we have found eight existing and stable phases and along the $D/q|J|$ -axis, three particular hybrid phases appear at the three multicritical points A_5 , A_6 and A_7 . The ground-state phase diagram is considered and used as a guide for obtaining different temperature phase diagrams. We also investigated the phase diagrams in the $(D/|J|, k_B T/|J|)$ plane, shown in figure 3. Then, in the presence and without

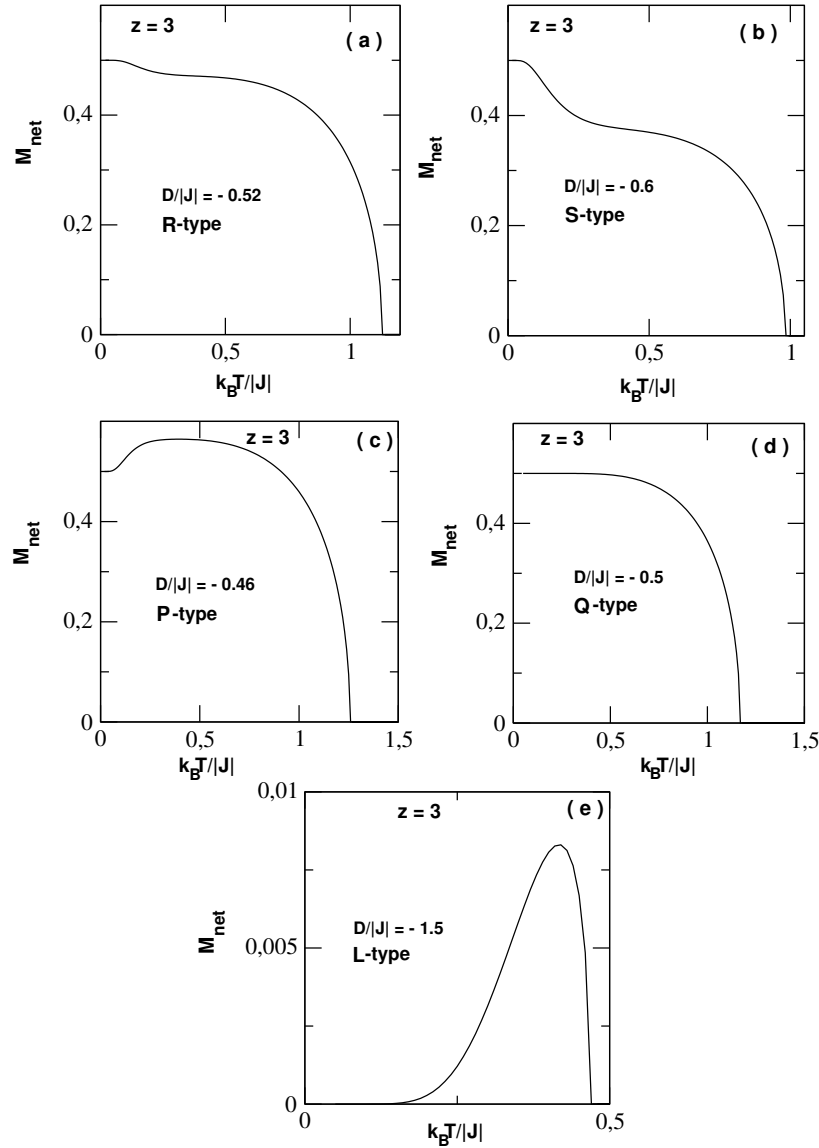


Figure 9. The Néel nomenclature of average magnetization: (a) R-type for $D/|J| = -0.52$; (b) S-type for $D/|J| = -0.6$; (c) P-type for $D/|J| = -0.46$; (d) Q-type for $D/|J| = -0.5$; (e) R-type for $D/|J| = -1.5$.

the longitudinal magnetic field h , we examined the thermal variations of the sublattice magnetizations, the global magnetization, the corresponding response functions and the internal energy as reported in figures 4–10. From these figures, the order-parameters in most cases showed a usual decay with thermal fluctuations. By using these behaviours and the analysis of the corresponding response functions and the internal energy, the nature of different phase transitions encountered is identified. The model shows rich physical properties, namely the second-order transition and multicritical points for all values of the crystal-field interactions and for all values of the coordination number z .

As a final note, it is useful to mention that different results achieved here are compared to those reported in some previous works [24, 51] and topological similarities are found.

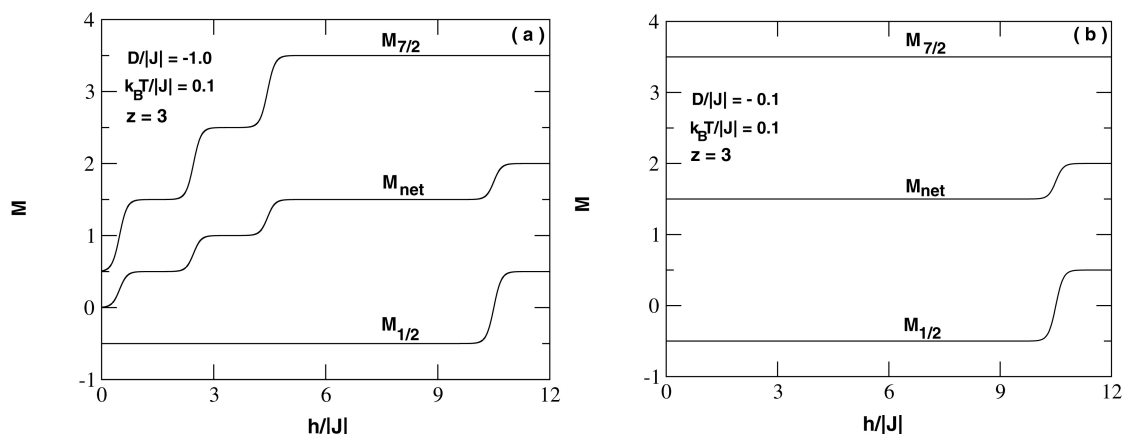


Figure 10. Magnetizations $M_{1/2}$, $M_{7/2}$ and M_{net} plotted as functions of the magnetic field h for selected values of the crystal-field when $z = 3$ as indicated in different panels.

References

- White R.M., Science, 1985, **229**, 11, doi:10.1126/science.229.4708.11.
- Wood R., Understanding Magnetism, Tab Books Inc.: Blue Ridge Summit, Pennsylvania, 1988.
- Köster E., J. Magn. Magn. Mater., 1988, **120**, 1, doi:10.1016/0304-8853(93)91274-B.
- Lueck L.B., Gilson R.G., J. Magn. Magn. Matter., 1990, **88**, 227, doi:10.1016/S0304-8853(97)90032-9.
- Itoh K., Kinoshita M., Molecular Magnetism: New Magnetic Materials, Kodansha and Gordon & Breach Science Publishers, Tokyo–Amsterdam, 2000.
- Linert W., Verdguer M. (Eds.), Molecular Magnets: Recent Highlights, Springer, Berlin, 2003.
- Gatteschi D., Adv. Mater., 1994, **6**, 635, doi:10.1002/adma.19940060903.
- Miller J.S., Epstein A.J., Chem. Eng. News, 1995, **73**, 30, doi:10.1021/cen-v073n040.p030.
- Kahn O., Molecular Magnetism, VCH Publishers, Inc., New York, 1993.
- Thompson C.J., Mathematical Statistical Mechanics, Princeton University Press, Princeton, New Jersey, 1992.
- Bobák A., Physica A, 1998, **258**, 140, doi:10.1016/S0378-4371(98)00233-7.
- Quadros S.G.A., Salinas S.R., Physica A, 1994, **206**, 479, doi:10.1016/0378-4371(94)90319-0.
- El Bouziani M., Gaye A., Jellal A., Physica A, 2013, **392**, 689, doi:10.1016/j.physa.2012.10.007.
- Da Cruz Filho J.S., Godoy M., Arruda A.S., Physica A, 2013, **392**, 6247, doi:10.1016/j.physa.2013.08.007.
- Miao H., Wei G., Geng J., J. Magn. Magn. Mater., 2009, **321**, 4139, doi:10.1016/j.jmmm.2009.08.018.
- Mohamad H.K., Domashevskaya E.P., Klinskikh A.F., Physica A, 2009, **388**, 4713, doi:10.1016/j.physa.2009.08.014.
- Mohamad H.K., Int. J. Adv. Res., 2014, **2**, 442.
- Kaneyoshi T., Chen J.C., J. Magn. Magn. Mater., **98**, 1991, 201, doi:10.1016/0304-8853(91)90444-F.
- Benyoussef A., El Kenz A., Kaneyoshi T., J. Magn. Magn. Mater., 1994, **131**, 179, doi:10.1016/0304-8853(94)90026-4.
- Bobák A., Jurčičin M., Physica A, 1997, **240**, 647, doi:10.1016/S0378-4371(97)00044-7.
- De Oliveira D.C., Silva A.A.P., de Albuquerque D.F., de Arruda A.S., Physica A, 2007, **386**, 205, doi:10.1016/j.physa.2007.07.073.
- Kaneyoshi T., Physica A, 1994, **205**, 677, doi:10.1016/0378-4371(94)90229-1.
- Guo K.-T., Xiang S.-H., Xu H.-Y., Li X.-L., Quantum Inf. Process., 2014, **13**, 1511, doi:10.1007/s11128-014-0745-7.
- Deviren B., Keskin M., Canko O., Physica A, 2009, **388**, 1835, doi:10.1016/j.physa.2009.01.032.
- Buendía G.M., Liendo J.A., J. Phys.: Condens. Matter, 1997, **9**, 5439, doi:10.1088/0953-8984/9/25/011.
- Godoy M., Figueiredo W., Phys. Rev. E, 2002, **66**, 036131, doi:10.1103/PhysRevE.66.036131.
- Cambuí D.S., de Arruda A.S., Godoy M., Int. J. Mod. Phys. C, 2012, **23**, 1240015, doi:10.1142/S0129183112400153.
- Feraoun A., Zaim A., Kerouad M., Physica B, 2014, **445**, 74, doi:10.1016/j.physb.2014.03.071.
- Žukovič M., Bobák A., J. Magn. Magn. Mater., 2010, **322**, 2868, doi:10.1016/j.jmmm.2010.04.043.
- Jiang W., Bai B.-D., Phys. Status Solidi B, 2006, **243**, 2892, doi:10.1002/pssb.200541244.

31. Essaoudi I., Bärner K., Ainane A., Saber M., Physica A, 2007, **385**, 208, doi:10.1016/j.physa.2007.06.037.
32. Yessoufou R.A., Bekhechi S., Hontinfinde F., Eur. Phys. J. B, 2011, **81**, 137, doi:10.1140/epjb/e2011-10825-7.
33. Kplé J., Yessoufou R.A., Hontinfinde F., Afr. Rev. Phys., 2012, **7**, 319.
34. Yigit A., Albayrak E., Chin. Phys. B, 2012, **21**, 020511, doi:10.1088/1674-1056/21/2/020511.
35. Ekiz C., Phys. Lett. A, 2007, **367**, 483, doi:10.1016/j.physleta.2007.03.038.
36. Albayrak E., Yigit A., Phys. Lett. A, 2006, **353**, 121, doi:10.1016/j.physleta.2005.12.077.
37. Karimou M., Yessoufou R., Hontinfinde F., Int. J. Mod. Phys. B, 2015, **29**, 1550194, doi:10.1142/S0217979215501945.
38. Ekiz C., J. Magn. Magn. Mater., 2006, **307**, 139, doi:10.1016/j.jmmm.2006.03.059.
39. Ekiz C., Commun. Theor. Phys., 2009, **52**, 539, doi:10.1088/0253-6102/52/3/30.
40. Strečka J., Jaščur M., Acta Phys. Slovaca, 2015, **65**, 235, [Preprint arXiv:1511.03031v2, 2015].
41. Jaščur M., Štubňa V., Szałowski K., Balcerzak T., J. Magn. Magn. Mater., 2016, **417**, 92, doi:10.1016/j.jmmm.2016.05.048.
42. Koyama K., Fujii H., Goto T., Fukuda H., Janssen Y., Physica B, 2001, **294–295**, 168, doi:10.1016/S0921-4526(00)00634-7.
43. Albertini F., Bolzoni F., Paoluzi A., Paretì L., Zannoni E., Physica B, 2001, **294**, 172, doi:10.1016/S0921-4526(00)00635-9.
44. Baxter R.J., Exactly Solvable Models in Statistical Mechanics, Academic Press, London, 1982.
45. Néel L., Ann. Phys. Paris, 1932, **18**, 5.
46. Néel L., Ann. Phys. Paris, 1948, **3**, 137.
47. Ekiz C., Strečka J., Jaščur M., Cent. Eur. J. Phys., 2009, **7**, 509, doi:10.2478/s11534-009-0043-7.
48. Chikazumi S., Physics of Ferromagnetism, Oxford University Press, Oxford, 1997.
49. Hovhannisyan V.V., Strečka J., Ananikian N.S., J. Phys.: Condens. Matter, 2016, **28**, 8, doi:10.1088/0953-8984/28/8/085401.
50. Yao X., Dong S., Yu H., Liu J., Phys. Rev. B, 2006, **74**, 134421, doi:10.1103/PhysRevB.74.134421.
51. Karimou M., Yessoufou R.A., Oke T.D., Kpadonou A., Hontinfinde F., Condens. Matter Phys., 2016, **19**, 33003, doi:10.5488/CMP.19.33003.

Дослідження методом ґратки Бете змішаної спін- $\frac{1}{2}$ та спін- $\frac{7}{2}$ моделі Ізінга в поздовжньому магнітному полі

С. Еддаґрі¹, М. Каріму², А. Разук^{1,3}, Ф. Гонтінінде^{2,4}, А. Бенюссєф^{5,6}

¹ Інститут математики і фізичних наук (IMSP), Республіка Бенін

² Університет Абомей-Калаві, фізичний факультет, Республіка Бенін

³ LMPHE, Факультет природничих наук, університет Мохаммеда V, Рабат, Марокко

⁴ Лабораторія фізики матеріалів, факультет наук і технологій, університет султана Муле Слімана, Марокко

⁵ Відділення фізики, полідисциплінарний факультет, університет султана Муле Слімана, Марокко

⁶ Академія наук і технологій Хассана II, Рабат, Марокко

Досліджено магнітні властивості змішаної спін- $\frac{1}{2}$ та спін- $\frac{7}{2}$ моделі Ізінга з кристалічним полем у поздовжньому магнітному полі на ґратці Браве з використанням точних рекурсивних співвідношень. Побудована фазова діаграма основного стану. Температурно-залежна фазова діаграма продемонстрована для випадку однорідного кристалічного поля на площині $(k_B T / |J|, D / |J|)$ при відсутності зовнішнього обмеження для координаційних чисел $z = 3, 4, 6$. Параметр порядку, відповідна функція відгуку і внутрішня енергія обчислені та вивчені детально для встановлення справжньої природи фазових меж і відповідних температур. Термічні зміни середньої намагніченості прокласифіковано відповідно до номенклатури Неля.

Ключові слова: модель Ізінга, намагніченість, функція відгуку, вільна енергія, фазова діаграма, перехід другого роду